

Bifunctional Electromagnetic Manipulation of Surface Waves Using Metasurfaces Under One Circularly Polarized Incidence

Min Kang , Lixing Chen, Shuai-peng Qin, Liang Ma, Aoxiang Rui and Shiqing Li *

Department of Applied Physics, Zhejiang University of Technology, Hangzhou 310023, China

* Correspondence: 211122090021@zjut.edu.cn (M.K.); sql@zjut.edu.cn (S.L.)

Abstract: The ability to freely manipulate the wavefronts of surface plasmon polaritons (SPPs) or surface waves (SWs), particularly with multifunctional integration, is of great importance in near-field photonics. However, conventional SPP control devices typically suffer from low efficiency and single-function limitations. Although recent works have proposed metasurfaces that achieve bifunctional SPP manipulation, their implementation relies on the excitations of circularly polarized (CP) light with different helicities. Here, we propose a generic approach to designing bifunctional SPP meta-devices under single-helicity circularly polarized incidence. Constructed using carefully selected and arranged meta-atoms that possess both structural resonance and a geometric phase, this kind of meta-device can exhibit two distinct SPP manipulation functionalities in both co- and cross-polarized output channels under one CP incidence. As proof of this concept, we designed a bifunctional meta-device in the microwave regime and numerically demonstrated that it can convert a normally incident left circularly polarized (LCP) beam into SWs, exhibiting both a focused wavefront in the co-polarized output channel and a deflected wavefront in the cross-polarized output channel. Our findings substantially enrich the capabilities of metasurfaces to manipulate near-field electromagnetic waves, which can find many applications in practice.

Keywords: bifunctional; metasurface; surface waves; co-polarized; cross-polarized



Received: 17 December 2024

Revised: 9 January 2025

Accepted: 17 January 2025

Published: 20 January 2025

Citation: Kang, M.; Chen, L.; Qin, S.; Ma, L.; Rui, A.; Li, S. Bifunctional Electromagnetic Manipulation of Surface Waves Using Metasurfaces Under One Circularly Polarized Incidence. *Photonics* **2025**, *12*, 91. <https://doi.org/10.3390/photronics12010091>

Copyright: © 2025 by the authors. Licensee MDPI, Basel, Switzerland. This article is an open access article distributed under the terms and conditions of the Creative Commons Attribution (CC BY) license (<https://creativecommons.org/licenses/by/4.0/>).

1. Introduction

Surface plasmon polaritons (SPPs), which are elementary excitations arising from the coupling of photons and free-electron oscillations at dielectric/metal interfaces, have garnered significant attention over the past few decades due to their wide range of applications in sub-diffraction-limit imaging, biological and chemical sensing, on-chip photonic circuits, and more [1,2]. In low-frequency regimes, where natural SPPs do not occur, spoof SPPs on structured metals offer equally intriguing possibilities for a variety of applications [3–7]. The ability to control these surface waves (SWs, including SPPs and spoof SPPs) is crucial for advancing near-field photonics.

During the last two decades, metasurfaces, which can locally provide abrupt phase shifts at subwavelength intervals to tailor the phase of the incident waves, have been proposed and have shown strong capabilities to manipulate EM waves with flat configurations, subwavelength sizes, and high efficiencies [8–12]. In response to linearly or circularly polarized (CP) waves, the phase responses of meta-atoms on these metasurfaces are dictated by either structural resonance [13,14] or the Pancharatnam–Berry (PB) mechanism [14,15]. Many fascinating wavefront manipulation effects have been discovered, including anomalous reflection/refraction [16,17], the photonic spin Hall effect [18–20],

meta-holograms [21–23], flat lenses [24,25], complex beam generation [26–30], spatial light modulation with multifunctionality [31–33], and many others [34–36]. Additionally, metasurfaces have also been proposed for converting PWs into SWs [37–40] and manipulating the wavefront of SWs [41–43]. However, despite the great successes already achieved with metasurfaces, the existing designs for achieving SPP excitation and wavefront manipulation still rely on separate devices for each functionality, limiting their integration into compact systems. Recently, polarization-controlled bifunctional metasurfaces for near-field SW manipulations have been proposed and experimentally demonstrated in both the microwave and optical regimes.

In this paper, we propose a high-efficiency bifunctional meta-device capable of simultaneously exciting SWs and manipulating their wavefronts under single-helicity circularly polarized incidence. Unlike previous works that require separate devices or operated under different helicities for each functionality, our approach integrates both functionalities into one metasurface under a single CP incidence. To validate the concept, we designed a microwave meta-device and numerically characterized its performance. By engineering a series of meta-atoms with tailored reflection phases, we constructed a meta-device with pre-designed phase profiles, enabling the conversion of an incident LCP plane wave into both a focused surface wave (SW) beam and a deflected SW beam in the co- and cross-polarized output channels (Figure 1). Our results pave the way for the realization of ultra-compact devices that integrate diverse functionalities for near-field manipulations, with potential applications in near-field sensing, imaging, and on-chip photonics.

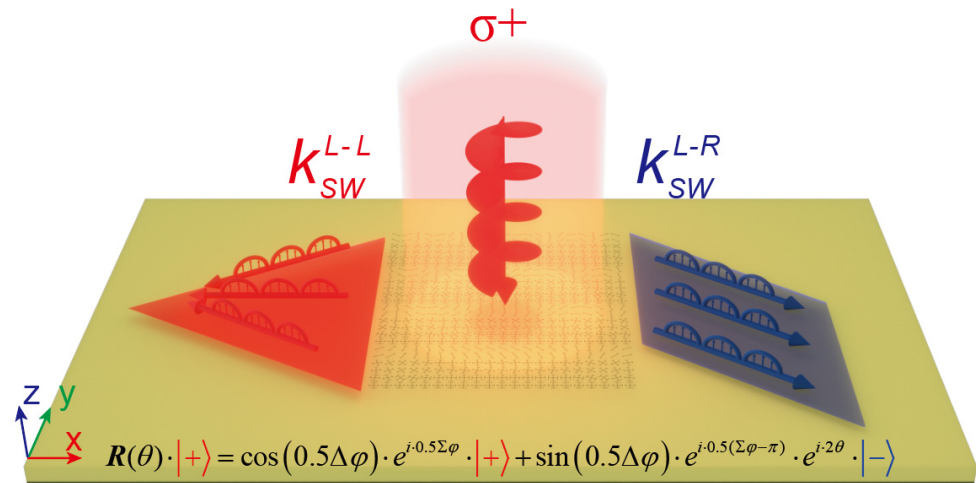


Figure 1. Schematic principle of proposed metasurfaces. Schematic of the designed bifunctional metasurface for near-field SW manipulations in both co- and cross-polarized output channels, as shined using single-helicity circularly polarized (CP) waves. The output SWs can achieve an arbitrary functionality, such as SWs with a focusing wavefront in the co-polarized output channel and SWs with a deflecting wavefront in the cross-polarized output channel.

2. The Physical Concept

We describe our strategy for designing a meta-device that exhibits bifunctional surface wave (SW) control, with distinct functionalities implemented in the co- and cross-polarized output channels under LCP wave incidence. We need to impose independent spatial functional wavefronts onto each output CP component. As discussed in Ref. [35], by introducing geometric phases and structural resonance, the electromagnetic energy carried by the co- and cross-polarized reflected fields can be fully phase-modulated with independent wavefronts, and the output can be described using the following equation:

$$R(\theta) \cdot |+\rangle = \cos(0.5\Delta\varphi) \cdot e^{i \cdot 0.5\Sigma\varphi} \cdot |+\rangle + \sin(0.5\Delta\varphi) \cdot e^{i \cdot 0.5(\Sigma\varphi - \pi)} \cdot e^{i \cdot 2\theta} \cdot |-\rangle \quad (1)$$

in which $R(\theta)$ represents the Jones matrix of each element with location (x, y) , θ represents the rotation angle of the meta-atom derived from the rotation matrix $M(\theta) = \begin{bmatrix} \cos\theta & \sin\theta \\ -\sin\theta & \cos\theta \end{bmatrix}$, $\Delta\varphi = \varphi_{xx} - \varphi_{yy}$ is the phase difference between two orthogonal linear polarizations, and $\Sigma\varphi = \varphi_{xx} + \varphi_{yy}$ is the phase summation of these two polarizations. The Jones matrix of the concerned reflective metasurface can be expressed as follows, $R(0) = \begin{bmatrix} r_{xx} & 0 \\ 0 & r_{yy} \end{bmatrix}$, where $r_{xx} = R_{xx}e^{i\varphi_{xx}}$ and $r_{yy} = R_{xx}e^{i\varphi_{yy}}$ represent the reflection coefficient of the x-pol and y-pol incident, respectively. The normal wave corresponds to the mirror reflection of the incident EM waves, while the anomalous wave results from the mutual interference of scattered light with the meta-atoms. Ignoring the absorption loss, the efficiencies of the normal and anomalous waves are $R_n = \cos^2(0.5\Delta\varphi)$ and $R_a = \sin^2(0.5\Delta\varphi)$, respectively. Obviously, the condition $0.5\Delta\varphi = \varphi_{xx} - \varphi_{yy} = \pi/4$ can ensure that the output LCP and RCP channels share an equal efficiency of 50%.

It can be observed in Equation (1) that there are theoretically two CP output components resulting from the LCP wave incidence. The co-polarized component retains the same CP state as the input $|+\rangle$, while the other exhibits the opposite polarization state $|-\rangle$, representing the cross-polarized output. The phase profile imprinted onto the co-polarized component, denoted as $\Phi_1 = 0.5\Sigma\varphi$, indicates that the wavefront of the co-polarized output can be directly tuned through phase summation of the two orthogonal linear polarizations, which is further adjusted according to the dimensions of the meta-atom. Meanwhile, the phase profile introduced in the cross-polarized field, which can be viewed as a geometric phase assisted by the propagation phase, is represented as $\Phi_2 = 0.5(\Sigma\varphi - \pi) + 2\theta$. The phase pattern of the co-polarized components ϕ_2 can be further determined according to the chirality-assisted phase, indicating that the cross-polarized components require an additional degree of freedom to decouple the inherent consistency between the co- and cross-polarized output channels. Moreover, the geometric phase influences only the cross-polarized field, $\phi_{PB} = \pm 2\theta$ (with \pm corresponding respectively to the LCP and RCP incident waves). In other words, the rotation angle associated with the geometric phase can be expressed as $\theta = \frac{1}{2}(\Phi_2 - \Phi_1 + \frac{\pi}{2})$.

In order to convert normally incident PWs into SWs with a specific wavefront, the metasurface needs to exhibit a specific phase profile. For example, if the phase profile is given by $\Phi(x, y) = \zeta_x x + k_{SW}(\sqrt{y^2 + F^2} - F)$ or $\Phi(x, y) = \zeta_x x + \zeta_y |y|$, where $\zeta_x > k_0$, with k_0 being the free-space wave vector, the generated SWs will acquire a wavefront of a focusing or Bessel beam. Now, our strategy is very clear: we need to design a metasurface, of which the co-polarized and cross-polarized output channels are imparted with the required phase profiles to generate SWs with a particular wavefront. Based on the analysis above, it can be inferred that we first need to design a series of meta-atoms so that their $0.5\Sigma\varphi$ values cover the entire 2π range. Meanwhile, by assigning different initial phases to the meta-atoms in each column, the resulting functions are combined to generate SWs with focusing beam profiles in the co-polarized output waves, while SWs with deflecting beam profiles in the cross-polarized output waves can be independently realized through additional rotation of the meta-atoms.

3. The Meta-Atom Designs

We choose the microwave regime for proving our scheme. The meta-atoms we designed are depicted in Figure 2a, which is a sandwich structure consisting of a metallic Jerusalem cross and a ground metallic plane, separated by a 1.5 mm thick dielectric spacer ($\epsilon_r = 3 + 0.01i$). The ground metallic plane blocks all transmissions through the system and, more importantly, couples with the metallic crosses to create magnetic resonances

at the frequencies dictated by the geometrical parameters [44,45]. Due to the presence of the metallic ground plate, these meta-atoms can completely reflect EM waves polarized along two cross directions (denoted as the x and y axes in the following) but with different reflection phases, φ_{xx} and φ_{yy} . Due to the resonance mechanism, the reflection phases φ_{xx} and φ_{yy} are primarily related to the dimensions of the meta-atom in the x -direction and the y -direction, respectively. Figures 2c and 2d, respectively, show the simulated $0.5\Delta\varphi$ and $0.5\Sigma\varphi$ values as a function of l_x ($l_x = l_1 + b_1$) and l_y ($l_y = l_2 + b_2$) at 10 GHz. To achieve bi-functional manipulation of both the co-polarized and cross-polarized output channels, a database of meta-atoms (with a period of 7 mm and a dielectric layer thickness of 1.5 mm) is established by varying the length l_x and the width l_y , as shown in these figures, to provide the necessary phase distributions for the required functionalities. Based on the analysis in the previous section, it is evident that under the input of the LCP wave, $0.5\Delta\varphi$ governs the energy ratio of the LCP and RCP output components, and $0.5\Sigma\varphi$ determines the phase imprinted onto the LCP output component. For simplicity, a series of meta-atoms at a working frequency of 10 GHz, as shown by the purple lines in Figure 2c, is chosen for constructing the metasurface, which possess the same $0.5\Delta\varphi = \pi/4$, ensuring that the output LCP and RCP channels share an equal amount of energy.

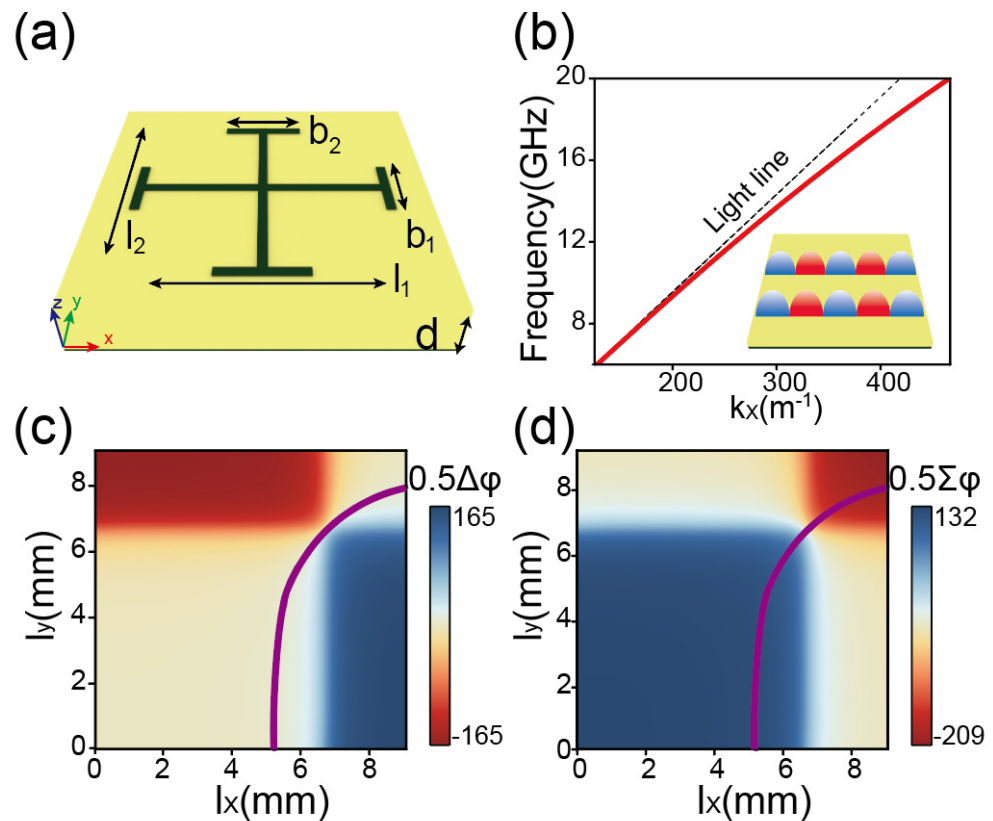


Figure 2. Characterization of the designed meta-atoms and plasmonic metal. (a) Geometry of the designed meta-atom (sized 7×7 mm²) composed of the metallic Jerusalem cross structure array and a flat metal mirror separated by a 1.5 mm thick dielectric spacer. (b) Finite element method (FEM)-simulated dispersion relation (red line) of the eigen SWs supported by the plasmonic metal, as depicted in the inset. (c,d) Pseudocolor maps of simulated (c) $0.5\Delta\varphi$ and (d) $0.5\Sigma\varphi$ for the structure of (a) in a parameter space spanned by l_x ($l_x = l_1 + b_1$) and l_y ($l_y = l_2 + b_2$) at 10 GHz. The purple lines indicate $0.5\Delta\varphi = \pi/4$.

It is worth noting that some of the functionalities to be implemented here are related to the control of the SWs; therefore, we design a “plasmonic metal” supporting the spoof SWs in the microwave regime, which is a metallic ground plane with a 1.5 mm thick

dielectric layer put on top of it (see the inset in Figure 2b). Figure 2b depicts the FEM-simulated dispersion relation of the SW modes supported by such a system, which exhibits an eigen wave vector $k_{SW} = 1.0245k_0$ with k_0 being the free-space wave vector at the frequency of 10 GHz. For a real metal at microwave frequencies, its absorption power (P_{ab}) can be calculated using $P_{ab} = \frac{1}{2}\sqrt{\pi u_0 f / \sigma} \int |H_t|^2 ds$ [46], where H_t (obtained in the PEC approximation) is the tangential component of the magnetic field on the metal's surface, σ is the metal's conductivity, f is the wave frequency, and s represents the metal's surface. Using this formula, we calculate the absorption power (P_a , caused by the metal) in the unit cell for the SSPPs and then evaluate the propagation length using $L = 1/2\alpha$, where $\alpha = P_a/2P_0$ and P_0 is the SSPP's power. The propagation length of the SSPP is found to be $L_{SSPP} = 113.64\lambda_0$.

4. Meta-Device Realizations: Microwave Simulations

With both the physical concept and the properties of our meta-atoms fully understood, we now use these meta-atoms to demonstrate a bifunctional meta-device that integrates both the focusing and deflecting effects of the SWs under LCP wave incidence at 10 GHz. The SW focusing beam can converge the electromagnetic waves to a single point, achieving high directivity. It is widely used in fields such as optical imaging and near-field microscopy, where precise control over the wave concentration is essential. On the other hand, the deflecting beam redirects the electromagnetic waves to a specific angle, offering fine control over the wave propagation. This is commonly applied in radar systems, beam steering, and other precision-guided technologies.

To achieve the bifunctional integration of SW focusing and deflection, the meta-device needs to exhibit the following chiral-dependent phase distributions under LCP wave incidence:

$$\begin{cases} \varphi^+(x, y) = 0.5\Sigma\varphi = -\xi_1 x + \xi_1 \left(\sqrt{y^2 + F^2} \right) \\ \varphi^-(x, y) = 0.5\Sigma\varphi + \sigma \cdot 2\theta(x, y) = -k_{sw} - k_{sw} \sin\theta \cdot y \end{cases} \quad (2)$$

where $\xi_1 = 1.071k_0$, $k_{SW} = 1.0245k_0$, $\theta = 60^\circ$, and $F = 200$ mm in this case that we are concerned with. According to our analyses presented in Section 1, as depicted in Figure 1, such a meta-device can convert a normally incident LCP beam ($\sigma = +$) into two separate beams: the co-polarized component is converted into an SW, which is then focused onto a point at a distance F away from the device's center, while the cross-polarized ($\sigma = -$) component is converted into an SW, which is reflected in an oblique direction at $\theta = 60^\circ$. We now employ the meta-atoms designed in Sec. 3 to construct this meta-device. To obtain the phase profile $\varphi^+(x, y)$ range coverage as accurately as possible, a library of 84 meta-atoms is meticulously established based on the cells indicated by the purple lines in Figure 2d.

The desired co- and cross-polarized phase profiles in Equation (2) are depicted in Figure 3a, respectively, with linear and parabolic phase profiles in the y -direction under LCP wave incidence. For the co-polarized output component, to achieve the required phase gradient ξ_1 in the x -direction, each column contains a set of four different meta-cells with an equal spacing in $0.5\Sigma\varphi$, arranged periodically. Specifically, the first column follows the sequence \dots , cell 1, cell 2, cell 3, cell 4, \dots , and the second row follows the pattern \dots , cell 5, cell 6, cell 7, cell 8, \dots . To obtain the desired parabolic phase profile in the y -direction, the $0.5\Sigma\varphi$ value of the meta-atom between each set (i.e., \dots , cell 9, cell 5, cell 1, cell 5, cell 9, \dots) follows a parabolic distribution. In general, the desired phase distribution of the co-polarized component determines the required sizes (l_x and l_y) of the meta-atoms at different positions. Then, by integrating the required phase distribution for the cross-polarized output component with the relationship $\phi_{PB} = 2\theta$, we can unambiguously determine the required orientation angles $\theta(x, y)$ of positions at different locations,

i.e., $\theta(x, y) = \left(-k_{SW} - k_{sw} \sin\theta \cdot y + \zeta_1 x - \zeta_1 \left(\sqrt{y^2 + F^2} \right) \right) / 2$. Ultimately, such a strategy guides us in designing our bifunctional metasurface, with the structural details displayed in Figure 3b–d.

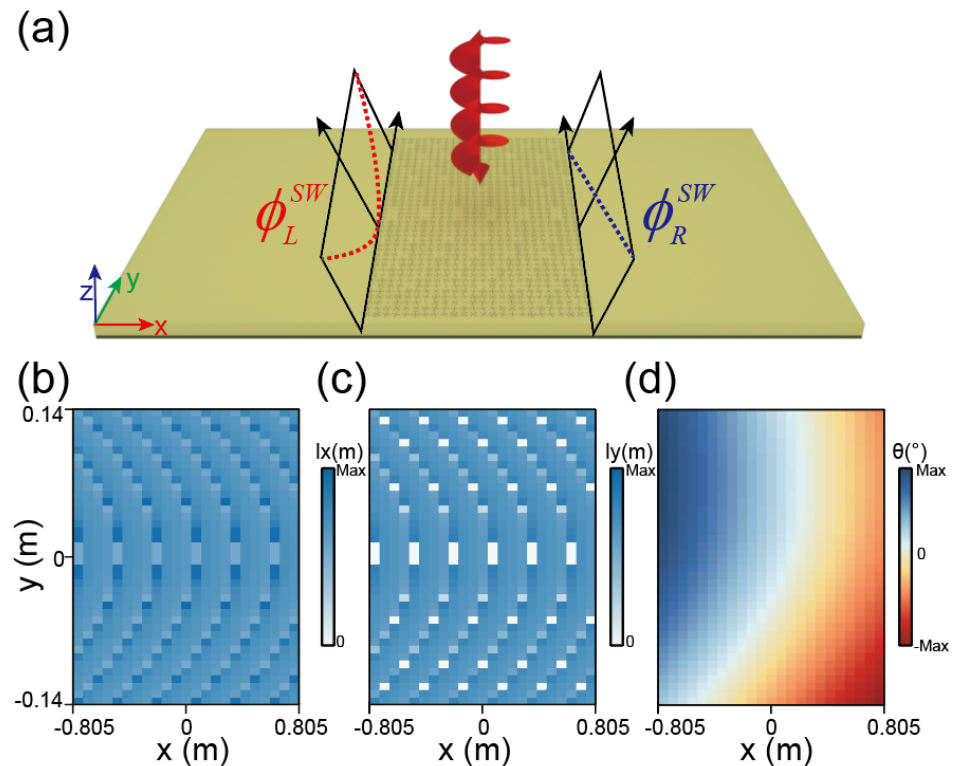


Figure 3. Structural details of the designed bifunctional meta–device. (a) The proposed meta–device for generating SWs with both hyperbolic and linear phase profiles dictated under LCP wave illumination. (b–d) Distributions of (b) $I_x(x, y)$, (c) $I_y(x, y)$, and (d) $\theta(x, y)$ of the designed bifunctional meta–device.

We next employed FEM simulations to validate our theoretical predictions. Figure 4a shows the simulated $\text{Re}[E_z]$ field distributions on a reference plane 1 mm above the whole device under LCP wave incidence. The simulated patterns clearly demonstrate that the incident LCP wave is first converted into SWs, which are then focused onto a focal point in the co-polarized output channel and deflected in the oblique direction in the cross-polarized output channel. Moreover, to characterize the performance of SW focusing further, Figure 4b presents the near-field $|E_y|^2 / |E_{y0}|^2$ distribution of the SWs at a numerically calculated focal length $F = 196$ mm, plotted against the y-coordinate, showing the excellent performance of the SW focusing beam. The other functionality, SW deflection, is also characterized by the $\text{Re}[E_z]$ field on the xy plane with $z = 1$ mm, as shown in Figure 4c. This result exhibits excellent agreement with the theoretical prediction, with the SWs being directed in the $\theta = 60^\circ$ direction. Notably, the desired co- and cross-polarized wave vector in Equation (2) with $\zeta_1 = 1.071k_0 = 1.04k_{SW}$ and k_{SW} . The eigen wave vector of the SW supported by the “plasmonic metal” is $k_{SW} = 1.0245k_0$ at this frequency. Although the wave vectors are not completely matched, the working efficiency of both output channels remains high. The FEM-simulated efficiencies of these two functionalities (i.e., SW focusing and SW deflection) are estimated as 40% and 37%, respectively. They are lower than the ideal value of 50%, which can be primarily attributed to the following reason: only spoof SWs with transverse-magnetic (TM) polarization exist on the designed “plasmonic metal”, while the incident CP wave contains both TM and transverse-electric (TE) components [47].

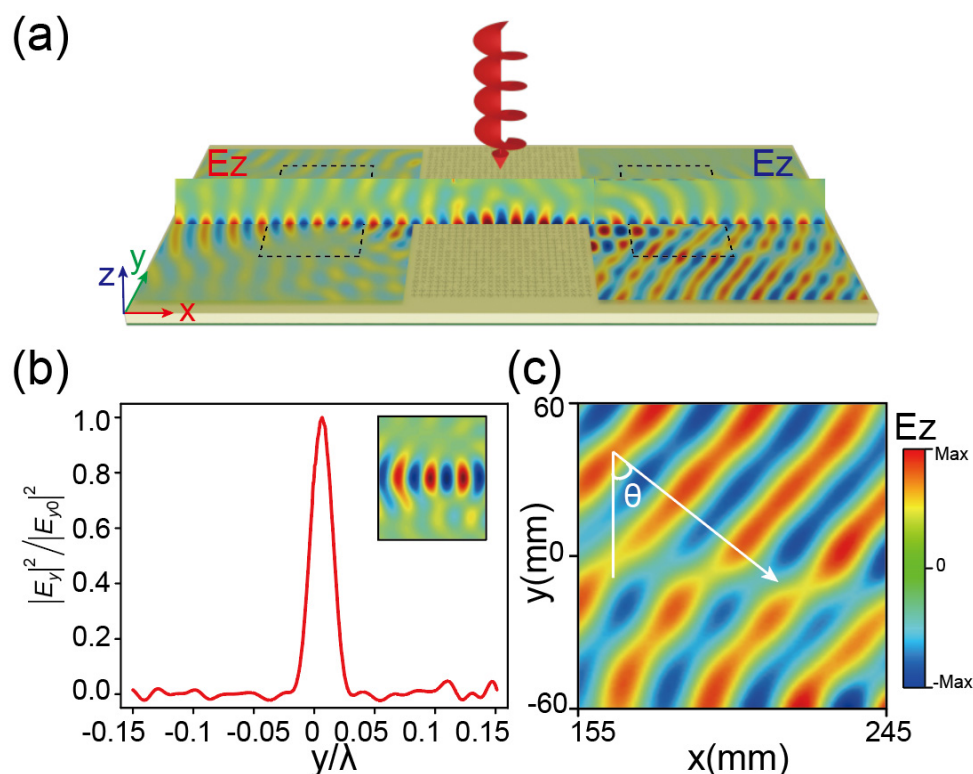


Figure 4. Bifunctional meta–device for near–field SW manipulations. (a) FEM–simulated near–field $\text{Re}[E_z]$ patterns in the whole system, as the meta–device is illuminated by an LCP wave. (b) The near–field $|E_y|^2/|E_{y0}|^2$ distribution of the SWs at the focal length position versus the y coordinate with $F = 196$ mm. The inset shows part of the SW focusing in the co–polarized output channel. (c) The simulated near–field $\text{Re}[E_z]$ profiles of the SW deflection in the cross–polarized output channel. Here, the frequency is fixed at 10 GHz.

5. Conclusions

In summary, we have proposed a novel approach that utilizes a single metasurface to simultaneously achieve bifunctional near-field manipulation of the SWs in reflection mode, under the excitation of an input circularly polarized wave with a specific helicity. By integrating two distinct mechanisms (the geometric phase and resonant mechanisms), the metasurface enables phase modulation for both the co-polarized and cross-polarized channels, thereby facilitating wavefront manipulation of the SWs. As a proof of concept, we carefully designed a meta-device and performed simulations that effectively validated the proposed scheme. Based on this design approach, the meta-device is capable of converting an incident LCP wave into focusing SWs in the co-polarized channel and deflecting SWs in the cross-polarized channel at 10 GHz. This method not only provides a compact solution for SW manipulation but also integrates both functionalities into one metasurface under a single CP incidence, which distinguishes it from previous designs that have typically required separate devices to realize different functionalities or operate diverse functionalities under different helicities. Our results open up a new avenue for the manipulation of surface waves using a single, ultra-compact meta-device, which combines small feature sizes with multifunctionality, making it well suited to future integrated optics applications.

Author Contributions: Conceptualization, S.L. and M.K.; methodology, M.K.; simulation, M.K., L.C., S.Q., L.M. and A.R. All authors have read and agreed to the published version of the manuscript.

Funding: This research was funded by the National Natural Science Foundation of China, grant number 12104401, and the Natural Science Foundation of Zhejiang Province, grant number LZ25A040002.

Institutional Review Board Statement: Not applicable.

Informed Consent Statement: Not applicable.

Data Availability Statement: The data that support the findings of this study are available from the corresponding author upon reasonable request.

Conflicts of Interest: The authors declare no conflicts of interest.

References

1. Raether, H. *Surface Plasmons on Smooth and Rough Surfaces and on Gratings*; Springer: Berlin/Heidelberg, Germany, 1988.
2. Barnes, W.L.; Dereux, A.; Ebbesen, T.W. Surface plasmon subwavelength optics. *Nature* **2003**, *424*, 824–830. [[CrossRef](#)] [[PubMed](#)]
3. Pendry, J.B.; Martín-Moreno, L.; García-Vidal, F.J. Mimicking surface plasmons with structured surfaces. *Science* **2004**, *305*, 847–848. [[CrossRef](#)]
4. Maier, S.A.; Andrews, S.R.; Martín-Moreno, L.; García-Vidal, F.J. Terahertz surface plasmon-polariton propagation and focusing on periodically corrugated metal wires. *Phys. Rev. Lett.* **2006**, *97*, 176805. [[CrossRef](#)]
5. Gan, Q.; Fu, Z.; Ding, Y.J.; Bartoli, F.J. Ultrawide-bandwidth slow-light system based on THz plasmonic graded metallic grating structures. *Phys. Rev. Lett.* **2008**, *100*, 256803. [[CrossRef](#)] [[PubMed](#)]
6. Lockyear, M.; Hibbins, A.; Sambles, J. Microwave surface-plasmon-like modes on thin metamaterials. *Phys. Rev. Lett.* **2009**, *102*, 73901. [[CrossRef](#)] [[PubMed](#)]
7. Zhang, H.C.; Liu, S.; Shen, X.; Chen, L.H.; Li, L.; Cui, T.J. Broadband amplification of spoof surface plasmon polaritons at microwave frequencies. *Laser Photonics Rev.* **2015**, *9*, 83–90. [[CrossRef](#)]
8. Sun, S.; He, Q.; Xiao, S.; Xu, Q.; Li, X.; Zhou, L. Gradient-index meta-surfaces as a bridge linking propagating waves and surface waves. *Nat. Mater.* **2012**, *11*, 426–431. [[CrossRef](#)] [[PubMed](#)]
9. Ni, X.; Emani, N.K.; Kildishev, A.V.; Boltasseva, A.; Shalae, V.M. Broadband light bending with plasmonic nanoantennas. *Science* **2012**, *335*, 427. [[CrossRef](#)]
10. Yu, N.; Genevet, P.; Kats, M.A.; Aieta, F.; Tetienne, J.-P.; Capasso, F.; Gaburro, Z. Light propagation with phase discontinuities: Generalized laws of reflection and refraction. *Science* **2011**, *334*, 333–337. [[CrossRef](#)] [[PubMed](#)]
11. Kowrdziej, R.; Ferraro, A.; Zografopoulos, D.C.; Caputo, R. Soft-Matter-Based Hybrid and Active Metamaterials. *Adv. Opt. Mater.* **2022**, *10*, 2200750. [[CrossRef](#)]
12. Lio, G.E.; Ferraro, A.; Zappone, B.; Parka, J.; Schab-Balcerzak, E.; Umeton, C.P.; Riboli, F.; Kowrdziej, R.; Caputo, R. Unlocking Optical Coupling Tunability in Epsilon-Near-Zero Metamaterials Through Liquid Crystal Nanocavities. *Adv. Opt. Mater.* **2023**, *12*, 2302483. [[CrossRef](#)]
13. Li, S.; Dong, S.; Yi, S.; Pan, W.; Chen, Y.; Guan, F.; Guo, H.; Wang, Z.; He, Q.; Zhou, L.; et al. Broadband and high-efficiency spin-polarized wave engineering with PB metasurfaces. *Opt. Express* **2020**, *28*, 15601–15610. [[CrossRef](#)] [[PubMed](#)]
14. Bomzon, Z.; Biener, G.; Kleiner, V.; Hasman, E. Space-variant Pancharatnam-Berry phase optical elements with computer-generated subwavelength gratings. *Opt. Lett.* **2002**, *27*, 1141–1143. [[CrossRef](#)] [[PubMed](#)]
15. Shitrit, N.; Bretner, I.; Gorodetski, Y.; Kleiner, V.; Hasman, E. Optical Spin Hall Effects in Plasmonic Chains. *Nano Lett.* **2011**, *11*, 2038–2042. [[CrossRef](#)] [[PubMed](#)]
16. Sun, S.; Yang, K.Y.; Wang, C.M.; Juan, T.-K.; Chen, W.T.; Liao, C.Y.; He, Q.; Xiao, S.; Kung, W.-T.; Guo, G.-Y.; et al. High efficiency broadband anomalous reflection by gradient meta-surfaces. *Nano Lett.* **2012**, *12*, 6223–6229. [[CrossRef](#)] [[PubMed](#)]
17. Grady, N.K.; Heyes, J.E.; Chowdhury, D.R.; Zeng, Y.; Reiten, M.T.; Azad, A.K.; Taylor, A.J.; Dalvit, D.A.R.; Chen, H.-T. Terahertz Metamaterials for Linear Polarization Conversion and Anomalous Refraction. *Science* **2013**, *340*, 1304–1307. [[CrossRef](#)]
18. Yin, X.; Ye, Z.; Rho, J.; Wang, Y.; Zhang, X. Photonic Spin Hall Effect at Metasurfaces. *Science* **2013**, *339*, 1405–1407. [[CrossRef](#)] [[PubMed](#)]
19. Luo, W.; Xiao, S.; He, Q.; Sun, S.; Zhou, L. Photonic Spin Hall Effect with Nearly 100% Efficiency. *Adv. Opt. Mater.* **2015**, *3*, 1102–1108. [[CrossRef](#)]
20. Luo, W.; Sun, S.; Xu, H.X.; He, Q.; Zhou, L. Transmissive Ultrathin Pancharatnam-Berry Metasurfaces with Nearly 100% Efficiency. *Phys. Rev. Appl.* **2017**, *7*, 044033. [[CrossRef](#)]
21. Zheng, G.; Mühlenbernd, H.; Kenney, M.; Li, G.; Zentgraf, T.; Zhang, S. Metasurface Holograms Reaching 80% Efficiency. *Nat. Nanotechnol.* **2015**, *10*, 308–312. [[CrossRef](#)]
22. Chen, W.T.; Yang, K.; Wang, C.; Huang, Y.-W.; Sun, G.; Chiang, I.-D.; Liao, C.Y.; Hsu, W.-L.; Lin, H.T.; Sun, S.; et al. High-Efficiency Broadband Meta-Hologram with Polarization-Controlled Dual Images. *Nano Lett.* **2014**, *14*, 225–230. [[CrossRef](#)]
23. Deng, Z.-L.; Deng, J.; Zhuang, X.; Wang, S.; Li, K.; Wang, Y.; Chi, Y.; Ye, X.; Xu, J.; Wang, G.P.; et al. Diatomic Metasurface for Vectorial Holography. *Nano Lett.* **2018**, *18*, 2885–2892. [[CrossRef](#)] [[PubMed](#)]

24. Chen, X.; Huang, L.; Mühlenbernd, H.; Li, G.; Bai, B.; Tan, Q.; Jin, G.; Qiu, C.-W.; Zhang, S.; Zentgraf, T. Dual-polarity plasmonic metalens for visible light. *Nat. Commun.* **2012**, *3*, 1198. [[CrossRef](#)]
25. Ding, X.; Monticone, F.; Zhang, K.; Zhang, L.; Gao, D.; Burokur, S.N.; de Lustrac, A.; Wu, Q.; Qiu, C.-W.; Alù, A. Ultrathin Pancharatnam-Berry metasurface with maximal cross-polarization efficiency. *Adv. Mater.* **2015**, *27*, 1195–1200. [[CrossRef](#)] [[PubMed](#)]
26. Li, S.; Tsakmakidis, K.L.; Jiang, T.; Shen, Q.; Zhang, H.; Yan, J.; Sun, S.; Shen, L. Unidirectional guided-wave-driven metasurfaces for arbitrary wavefront control. *Nat. Commun.* **2024**, *15*, 5992. [[CrossRef](#)]
27. Genevet, P.; Yu, N.; Aieta, F.; Kats, M.A.; Blanchard, R.; Gaburro, Z.; Capasso, F. Ultra-thin plasmonic optical vortex plate based on phase discontinuities. *Appl. Phys. Lett.* **2012**, *100*, 013101. [[CrossRef](#)]
28. Wang, Z.; Dong, S.; Luo, W.; Jia, M.; Liang, Z.; He, Q.; Sun, S.; Zhou, L. High-efficiency generation of Bessel beams with transmissive metasurfaces. *Appl. Phys. Lett.* **2018**, *112*, 191901. [[CrossRef](#)]
29. Pfeiffer, C.; Grbic, A. Controlling vector Bessel beams with metasurfaces. *Phys. Rev. Appl.* **2014**, *2*, 044012. [[CrossRef](#)]
30. Mehmood, M.Q.; Mei, S.; Hussain, S.; Huang, K.; Siew, S.Y.; Zhang, L.; Zhang, T.; Ling, X.; Liu, H.; Teng, J.; et al. Visible-frequency metasurface for structuring and spatially multiplexing optical vortices. *Adv. Mater.* **2016**, *28*, 2533–2539. [[CrossRef](#)] [[PubMed](#)]
31. Huang, Y.; Xiao, T.; Chen, S.; Xie, Z.; Zheng, J.; Zhu, J.; Su, Y.; Chen, W.; Liu, K.; Tang, M.; et al. All-optical controlled-NOT logic gate achieving directional asymmetric transmission based on metasurface doublet. *Opto-Electron. Adv.* **2023**, *6*, 220073. [[CrossRef](#)]
32. Zhang, F.; Pu, M.; Li, X.; Ma, X.; Guo, Y.; Gao, P.; Yu, H.; Gu, M.; Luo, X. Extreme-Angle Silicon Infrared Optics Enabled by Streamlined Surfaces. *Adv. Mater.* **2021**, *33*, 2008157. [[CrossRef](#)] [[PubMed](#)]
33. Zhang, F.; Guo, Y.; Pu, M.; Chen, L.; Xu, M.; Liao, M.; Li, L.; Li, X.; Ma, X.; Luo, X. Meta-optics empowered vector visual cryptography for high security and rapid decryption. *Nat. Commun.* **2023**, *14*, 1946. [[CrossRef](#)] [[PubMed](#)]
34. Dong, S.; Li, S.; Ling, X.; Hu, G.; Li, Y.; Zhu, H.; Zhou, L.; Sun, S. Broadband spin-unlocked metasurfaces for bifunctional wavefront manipulations. *Appl. Phys. Lett.* **2022**, *120*, 180404. [[CrossRef](#)]
35. Yuan, Y.; Sun, S.; Chen, Y.; Zhang, K.; Ding, X.; Ratni, B.; Wu, Q.; Burokur, S.N.; Qiu, C.-W. A fully phase-modulated metasurface as an energy-controllable circular polarization router. *Adv. Sci.* **2020**, *7*, 2001437. [[CrossRef](#)] [[PubMed](#)]
36. Yu, N.; Genevet, P.; Aieta, F.; Kats, M.A.; Blanchard, R.; Aoust, G.; Tétienne, J.-P.; Gaburro, Z.; Capasso, F. Flat optics: Controlling wavefronts with optical antenna metasurfaces. *IEEE J. Sel. Top. Quantum Electron.* **2013**, *19*, 4700423.
37. Huang, L.; Chen, X.; Bai, B.; Tan, Q.; Jin, G.; Zentgraf, T.; Zhang, S. Helicity dependent directional surface plasmon polariton excitation using a metasurface with interfacial phase discontinuity. *Light Sci. Appl.* **2013**, *2*, e70. [[CrossRef](#)]
38. Pors, A.; Nielsen, M.G.; Bernardin, T.; Weeber, J.C.; Bozhevolnyi, S.I. Efficient unidirectional polarization-controlled excitation of surface plasmon polaritons. *Light Sci. Appl.* **2014**, *3*, e197. [[CrossRef](#)]
39. Sun, W.; He, Q.; Sun, S.; Zhou, L. High-efficiency surface plasmon meta-couplers: Concept and microwave-regime realizations. *Light Sci. Appl.* **2016**, *5*, e16003. [[CrossRef](#)]
40. Li, S.; Wang, Z.; Dong, S.; Yi, S.; Guan, F.; Chen, Y.; Guo, H.; He, Q.; Zhou, L.; Sun, S. Helicity-Delinked Manipulations on Surface Waves and Propagating Waves by Metasurfaces. *Nanophotonics* **2020**, *9*, 3473–3481. [[CrossRef](#)]
41. Wang, Z.; Li, S.; Zhang, X.; Feng, X.; Wang, Q.; Han, J.; He, Q.; Zhang, W.; Sun, S.; Zhou, L. Excite spoof surface plasmons with tailored wavefronts using high-efficiency terahertz metasurfaces. *Adv. Sci.* **2020**, *7*, 2000982. [[CrossRef](#)]
42. Li, S.; Tu, W.; Zhang, H.; Yan, J.; Shen, L. Surface wave control via unidirectional surface magnetoplasmon waveguide arrays. *Opt. Mater. Express* **2024**, *14*, 996–1007. [[CrossRef](#)]
43. Dong, S.; Zhang, Y.; Guo, H.; Duan, J.; Guan, F.; He, Q.; Zhao, H.; Zhou, L.; Sun, S. Highly Efficient Wave-Front Reshaping of Surface Waves with Dielectric Metawalls. *Phys. Rev. Appl.* **2018**, *9*, 4032. [[CrossRef](#)]
44. Sievenpiper, D.; Broas, R.F.J.; Alexopoulos, N.G.; Yablonovitch, E. High-Impedance Electromagnetic Surfaces with a Forbidden Frequency Band. *Microw. Theory Tech. IEEE Trans.* **1999**, *47*, 2059. [[CrossRef](#)]
45. Hao, J.M.; Zhou, L.; Chan, C.T. An effective-medium model for high-impedance surfaces. *Appl. Phys. A* **2007**, *87*, 281–284. [[CrossRef](#)]
46. Kong, J.A. *Electromagnetic Wave Theory*; EMW Publishing: Boston, MA, USA, 2008.
47. Duan, J.; Guo, H.; Dong, S.; Cai, T.; Luo, W.; Liang, Z.; He, Q.; Zhou, L.; Sun, S. High-efficiency chirality-modulated spoof surface plasmon meta-coupler. *Sci. Rep.* **2017**, *7*, 1354. [[CrossRef](#)]

Disclaimer/Publisher’s Note: The statements, opinions and data contained in all publications are solely those of the individual author(s) and contributor(s) and not of MDPI and/or the editor(s). MDPI and/or the editor(s) disclaim responsibility for any injury to people or property resulting from any ideas, methods, instructions or products referred to in the content.